Supporting information for

Improved Phase Stability of γ-$CsPbI_3$ Perovskite Nanocrystals by Interface Effect using Iodine Modified Graphene Oxide

Qi Zhang[1], Yangying Zhou[1], Yaxuan Wei[1], Meiqian Tai[1], Hui Nan[1], Youchen Gu[1], Jianhua Han[1], Xuewen Yin[1], Jianbao Li[2,1] and Hong Lin[1]*

[1] State Key Laboratory of New Ceramics & Fine Processing, School of Materials Science and Engineering, Tsinghua University, Beijing 100084, China

[2] State Key Laboratory of Marine Resource Utilization in South China Sea, Materials and Chemical Engineering Institute, Hainan University, Haikou 570228, China

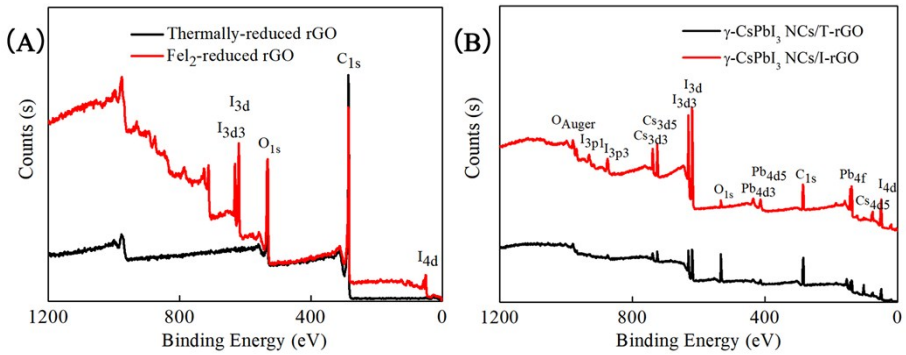

Figure S1. XPS spectra of (A) thermally-reduced rGO (T-rGO) and FeI_2-reduced rGO (I-rGO) and (B) γ-$CsPbI_3$ NCs/T-rGO and γ-$CsPbI_3$ NCs/I-rGO heterostructures.

Table S1. Element contents derived from the corresponding XPS spectra of thermally-reduced rGO, FeI_2-reduced rGO, γ-$CsPbI_3$ NCs/T-rGO and γ-$CsPbI_3$ NCs/I-rGO heterostructures.

	Thermally-reduced rGO, Atomic %	FeI_2-reduced rGO, Atomic %	γ-$CsPbI_3$ NCs/T-rGO, Atomic %	γ-$CsPbI_3$ NCs/I-rGO, Atomic %
C1s	84.47	72.36	64.68	66.33
N1s	0.84	0.95	3.84	2.79
O1s	14.52	20.69	25.45	8.48
Fe2p	0.18	4.59	-	-
I3d	-	1.41	3.84	14.81
Pb 4f	-	-	1.2	3.53
Cs 3d	-	-	0.99	4.05

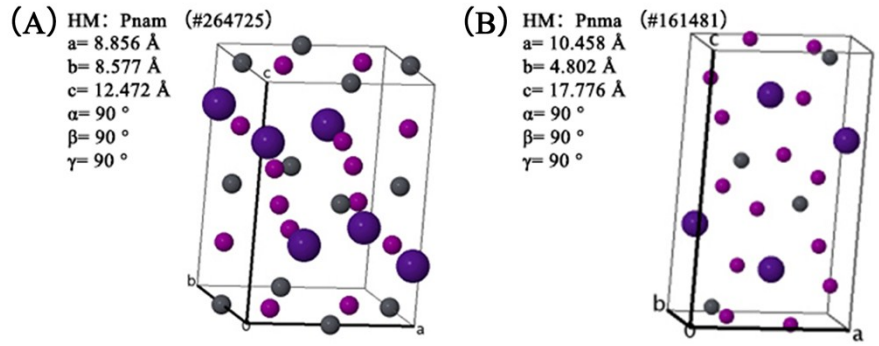

Figure S2. Schematic and structural parameters of γ-$CsPbI_3$ (ICSD #264725) and *δ*-$CsPbI_3$ (ICSD #161480).

As the formation of *γ*-$CsPbI_3$ NCs can be described as that Cs-oleate, Pb-oleate and iodine-organic amine (such as oleylammonium iodine (OAmI)) precursors grow through self-assembly and oriented attachment into NCs, OAmI precursors can act as a fundamental unit to assemble γ-$CsPbI_3$ NCs and manipulate the phase structure, morphology and crystals size of NCs. This variation can also be described by the different crystal structure of γ-$CsPbI_3$ and *δ*-$CsPbI_3$, which is shown in **Figure S2**. The standard γ-$CsPbI_3$ outlines an atomic ratio of Cs:Pb:I with 1:1:3, but exceed amount of Pb-oleate or OAmI could destroy this pseudo-cubic phase structure and give rise to the formation of *δ*-$CsPbI_3$.

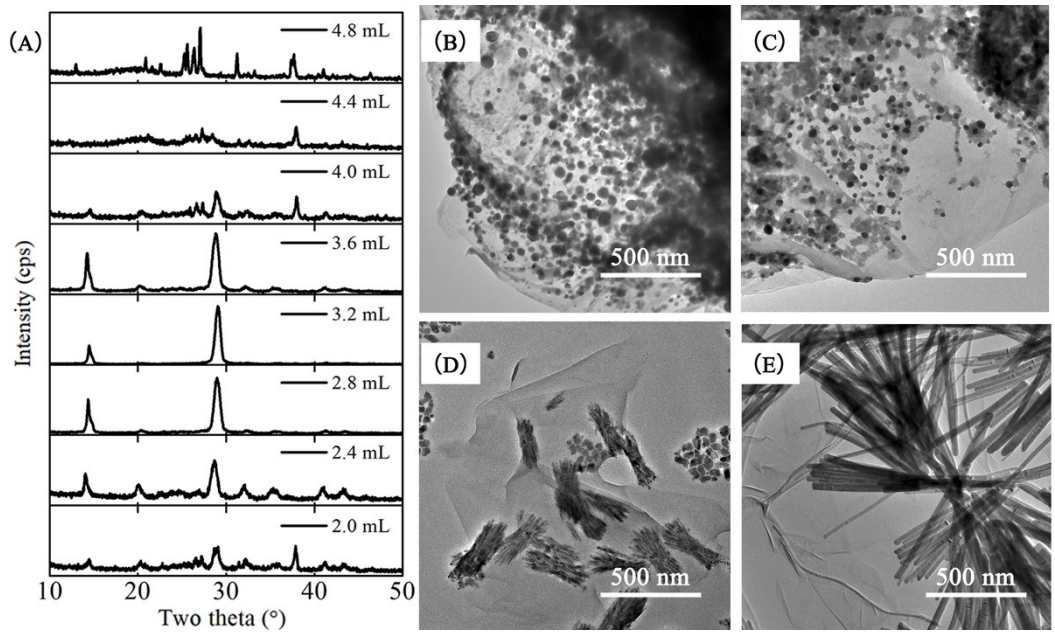

Figure S3. Structure and morphology of *γ*-$CsPbI_3$ NCs/rGO heterostructures with varying OAm added amounts. (A) XRD patterns of *γ*-$CsPbI_3$ NCs/rGO heterostructures with varying OAm

added amounts ranging from 2.0 to 2.4, 2.8, 3.2, 3.6, 4.0, 4.4, and 4.8 mL. (B-E) TEM images of γ-$CsPbI_3$ NCs/rGO heterostructures with OAm added amounts of (B) 2.0, (C) 2.8, (D) 4.0, and (E) 4.8 mL. The optimized OAm added amounts were 2.8-3.6 mL.

For OAm added amount essentially produces a large amount of OAmI precursors and then participate in the formation of γ-$CsPbI_3$ NCs, it is necessary to control OAm added amounts. The structure and morphology of γ-$CsPbI_3$ NCs/rGO heterostructures with varying OAm amounts are shown in **Figure S3**. Within the range of 2.4-3.6 mL, these γ-$CsPbI_3$ NCs showed only the (020) and (040) diffraction peaks in the XRD patterns (see **Figure S3(A)**) and a regular cubic-shape and a well-distribution on the surface of rGO (see **Figure S3(C)**).

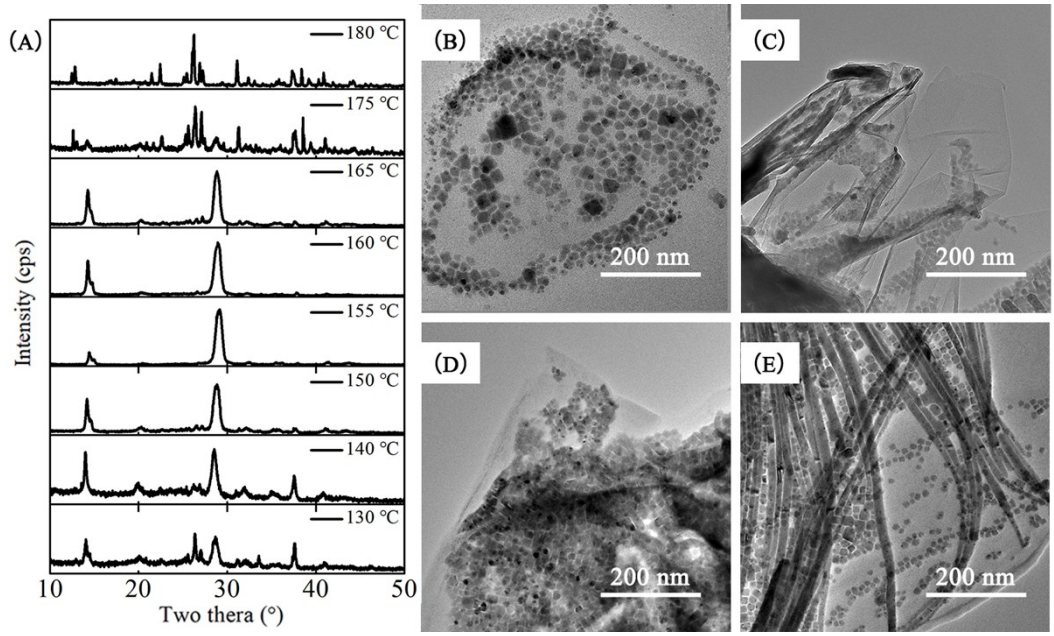

Figure S4. Structure and morphology of γ-$CsPbI_3$ NCs/rGO heterostructures with varying synthesis temperatures. (A) XRD patterns of γ-$CsPbI_3$ NCs/rGO heterostructures with varying synthesis temperatures ranging from 130 to 140, 150, 155, 160, 165, 175, and 180 °C. (B-E) TEM images of γ-$CsPbI_3$ NCs/rGO heterostructures with the synthesis temperatures of (B) 140, (C) 150, (D) 155, and (E) 175 °C. The optimized synthesis temperature were controlled between 150 and 165 °C.

Furthermore, synthesis temperature could obviously adjust these active precursors amounts, thus dominating the formation and quality of γ-$CsPbI_3$ NCs. The structure and morphology of γ-$CsPbI_3$ NCs/rGO heterostructures were also controlled by synthesis temperatures, as shown in **Figure S4**. When the synthesis temperature were controlled between 150 and 165 °C, γ-$CsPbI_3$ NCs/rGO heterostructures could obtain a high quality of γ-$CsPbI_3$ NCs, thus benefiting for improving their phase stability and optoelectronic properties.

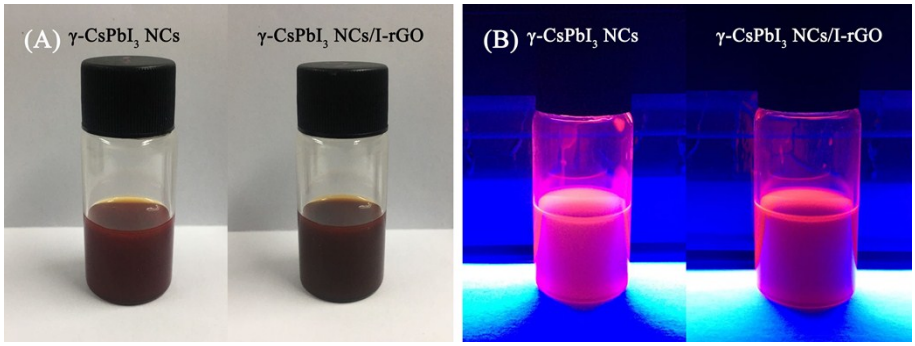

Figure S5. Samples of γ-$CsPbI_3$ NCs and γ-$CsPbI_3$ NCs/I-rGO in n-hexane under ambient and UV light.

Table S2. Morphology parameters derived from the corresponding TEM and HRTEM images of γ-$CsPbI_3$ NCs/*x*-rGO heterostructure films with varying rGO concentrations from 0 to 0.5 $g \cdot L^{-1}$.

	Lattice fringes, Å	Average crystal size, nm
γ-$CsPbI_3$ NCs	3.21	10.05
γ-$CsPbI_3$ NCs/0.1-rGO	3.24	11.25
γ-$CsPbI_3$ NCs/0.2-rGO	3.26	12.12
γ-$CsPbI_3$ NCs/0.3-rGO	3.27	12.56
γ-$CsPbI_3$ NCs/0.4-rGO	3.29	13.00
γ-$CsPbI_3$ NCs/0.5-rGO	3.32	16.81

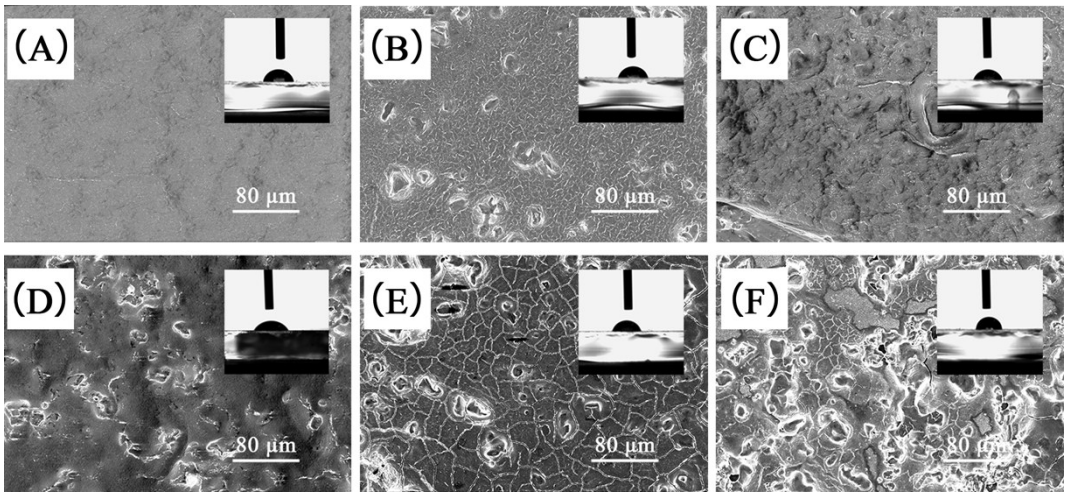

Figure S6. FE-SEM of γ-$CsPbI_3$ NCs/x-rGO heterostructures films with varying rGO concentrations of (A) 0, (B) 0.1, (C) 0.2, (D) 0.3, (E) 0.4 and (F) 0.5g·L^{-1}. The insets in **Figure S5(A-F)** show the contact angle of deionized water on the surface of γ-$CsPbI_3$ NCs/x-rGO heterostructure films. The corresponding contact angle range from 76.52 ° to 74.17 °, 70.31 °, 57.58 °, 73.47 ° and 87.99 °, respectively. With the increase of rGO concentration, small hole and crackle appeared on the surface of films and thus decreasing their contact angle. However, when rGO concentration exceed 0.4 g·L^{-1}, the film quality was serious degraded and excess rGO exposed to the surface of films and thus increasing their contact angle.

Table S3. Structural parameters derived from the corresponding XRD patterns of γ-$CsPbI_3$ NCs/*x*-rGO heterostructure films with varying rGO concentrations from 0 to 0.5 $g \cdot L^{-1}$, and stored in ambient conditions (room temperature of 25 °C and a humidity of 25% RH conditions) for 0 and 4 weeks without encapsulation. The crystal sizes of γ-$CsPbI_3$ NCs are calculated by Debye-Scherrer equation. (Instrument correction value for instrumental broadening changes =0.1252 °)

	XRD (0 week)			XRD (4 weeks)		
	Peak position of (040) Peak, °	Full width at half maximum of (040) Peak, °	Calculated crystal size, nm	Peak position of (040) Peak, °	Full width at half maximum of (040) Peak, °	Calculated crystal size, nm
γ-$CsPbI_3$ NCs	28.57	0.87	10.64	-	-	-
γ-$CsPbI_3$ NCs/0.1-rGO	28.56	0.80	11.76	28.45	0.60	16.62
γ-$CsPbI_3$ NCs/0.2-rGO	28.50	0.79	11.83	28.44	0.74	12.83
γ-$CsPbI_3$ NCs/0.3-rGO	28.49	0.76	12.38	28.43	0.75	12.61
γ-$CsPbI_3$ NCs/0.4-rGO	28.48	0.74	12.90	28.41	0.70	13.84
γ-$CsPbI_3$ NCs/0.5-rGO	28.48	0.60	16.80	-	-	-

Table S4. Optoelectronic parameters derived from the corresponding steady-state PL spectra and

time-resolved PL spectra of γ-$CsPbI_3$ NCs/x-rGO heterostructures films with varying rGO concentrations from 0 to 0.5 $g \cdot L^{-1}$. Time-resolved PL spectra of γ-$CsPbI_3$ NCs/x-rGO heterostructures were stored in ambient conditions for 0 and 4 weeks without encapsulation.

	Steady-state PL	Time-resolved PL (0 week)				Time-resolved PL (4 weeks)			
	Peak Position, nm	τ_1, ns	τ_2, ns	τ_3, ns	τ_{aver}, ns	τ_1, ns	τ_2, ns	τ_3, ns	τ_{aver}, ns
γ-$CsPbI_3$ NCs	706.00	10.09	29.59	104.92	32.10	-	-	-	-
γ-$CsPbI_3$ NCs/0.1-rGO	695.00	11.77	43.07	122.60	55.27	9.53	10.00	99.41	40.09
γ-$CsPbI_3$ NCs/0.2-rGO	688.00	12.29	45.28	125.48	67.77	10.93	39.01	111.17	49.39
γ-$CsPbI_3$ NCs/0.3-rGO	688.00	23.93	65.07	185.98	68.30	17.87	51.97	181.67	58.61
γ-$CsPbI_3$ NCs/0.4-rGO	686.00	10.25	38.67	130.22	51.40	7.68	29,21	111.40	33.89
γ-$CsPbI_3$ NCs/0.5-rGO	683.00	9.06	36.96	97.18	44.35	4.02	20.31	73.43	17.72

Table S5. PLQYs of γ-$CsPbI_3$ NCs/x-rGO heterostructures films with varying rGO concentrations from 0 to 0.5 $g \cdot L^{-1}$, and stored in ambient conditions for 4 weeks without encapsulation.

	0 week, %	1 week, %	2 weeks, %	3 weeks, %	4 weeks, %
γ-$CsPbI_3$ NCs	11.22	6.11	3.53	0.86	0.18
γ-$CsPbI_3$ NCs/0.1-rGO	11.01	6.86	3.92	3.22	1.57
γ-$CsPbI_3$ NCs/0.2-rGO	10.74	10.22	9.43	8.34	7.28
γ-$CsPbI_3$ NCs/0.3-rGO	10.50	10.13	9.78	9.12	8.27
γ-$CsPbI_3$ NCs/0.4-rGO	9.48	8.36	7.28	4.27	3.56
γ-$CsPbI_3$ NCs/0.5-rGO	8.76	5.21	3.83	1.34	0.7